PROTOCOL

Deep Immunophenotyping of Human Whole Blood by Standardized Multi-parametric Flow Cytometry Analyses

Jian Gao[1,2] · Yali Luo[1,2] · Helian Li[1,2] · Yiran Zhao[1,2] · Jialin Zhao[1,2] · Xuling Han[1,2] · Jingxuan Han[1,2] · Huiqin Lin[1] · Feng Qian[1,2,3]

Abstract

Immunophenotyping is proving crucial to understanding the role of the immune system in health and disease. High-throughput flow cytometry has been used extensively to reveal changes in immune cell composition and function at the single-cell level. Here, we describe six optimized 11-color flow cytometry panels for deep immunophenotyping of human whole blood. A total of 51 surface antibodies, which are readily available and validated, were selected to identify the key immune cell populations and evaluate their functional state in a single assay. The gating strategies for effective flow cytometry data analysis are included in the protocol. To ensure data reproducibility, we provide detailed procedures in three parts, including (1) instrument characterization and detector gain optimization, (2) antibody titration and sample staining, and (3) data acquisition and quality checks. This standardized approach has been applied to a variety of donors for a better understanding of the complexity of the human immune system.

Keywords Deep immunophenotyping · Multi-parametric flow cytometry · Human whole blood · Gating strategies · Standardization
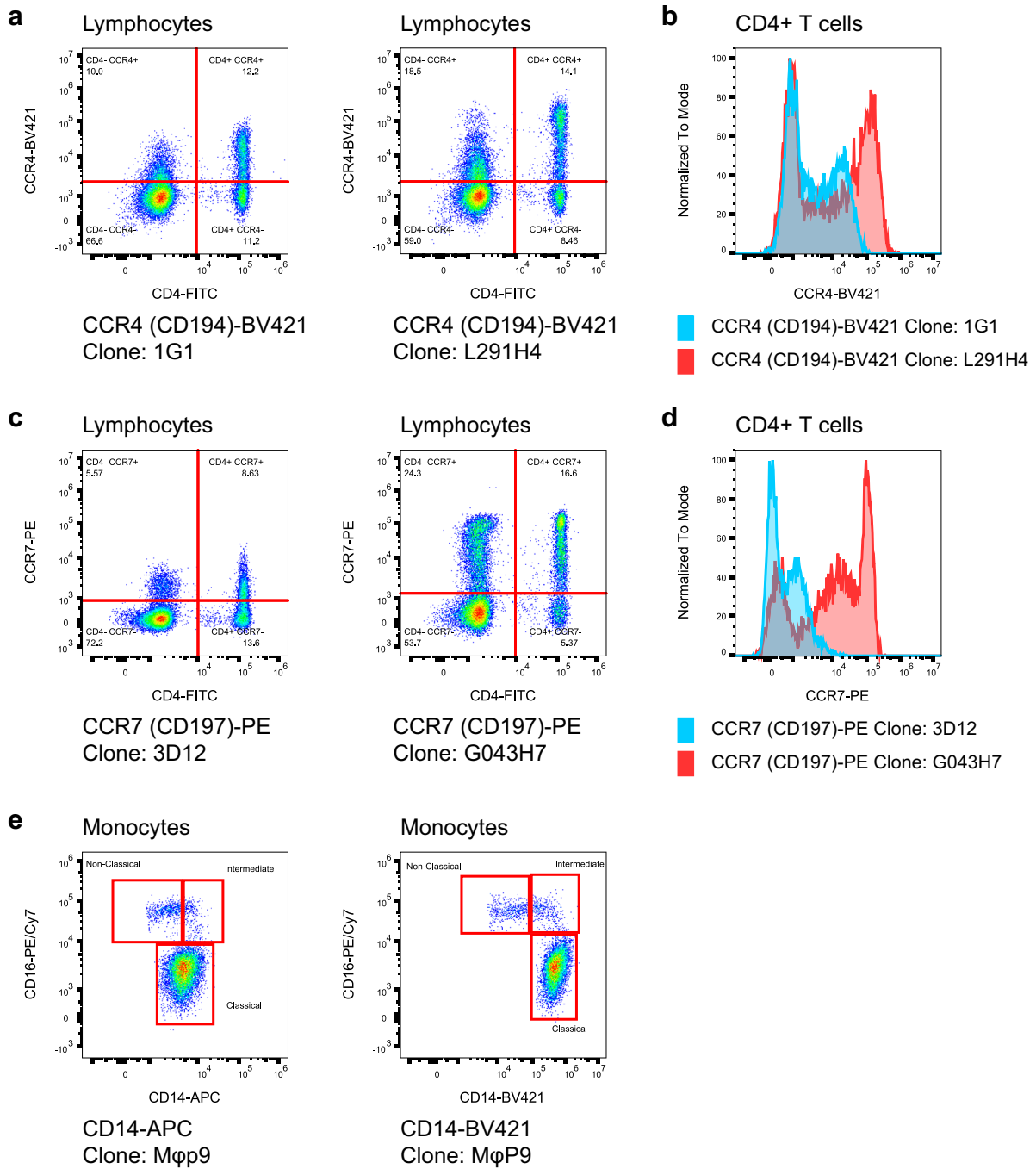
Abbreviations

AF	Alexa Fluor
APC	Allophycocyanin
BV	Brilliant Violet
CCPs	Negative control compensation particles
CCR	C–C motif chemokine receptor
CD	Cluster of differentiation
CM	Central memory
CXCR	C–X–C motif chemokine receptor
Cy5.5	Cyanine 5.5
Cy7	Cyanine 7
DCs	Dendritic cells
EDTA	Ethylenediaminetetraacetic acid
Eff/mem	Effector/memory
EM	Effector memory
FBS	Fetal bovine serum
FITC	Fluorescein isothiocyanate
FMO	Fluorescence minus one
FSC	Forward scatter
FSC-A	FSC-area
FSC-H	FSC-height
FSC-W	FSC-width
HIPC	Human Immunology Project Consortium
HLA-DR	Human leukocyte antigen-DR isotype
ICOS	Inducible T-cell costimulator
Ig	Immunoglobulin
LIN	Lineage
LLOQ	Lower limit of quantification
LOD	Limits of detection
MAIT cells	Mucosal-associated invariant T cells
mDCs	Myeloid dendritic cells
MFI	Median fluorescence intensity
NK cells	Natural killer cells
NKG2D	Natural killer group 2 member D
NKp46	Natural killer cell p46-related protein

✉ Feng Qian
 fengqian@fudan.edu.cn

1 State Key Laboratory of Genetic Engineering, Shanghai Public Health Clinical Center, Human Phenome Institute, Zhangjiang Fudan International Innovation Center and School of Life Sciences, Fudan University, Shanghai 200438, China

2 Ministry of Education Key Laboratory of Contemporary Anthropology, School of Life Sciences, Fudan University, Shanghai 200438, China

3 Institute of Immunophenome, International Human Phenome Institutes (Shanghai), Shanghai 200433, China

a

Lymphocytes

CCR4 (CD194)-BV421
Clone: 1G1

Lymphocytes

CCR4 (CD194)-BV421
Clone: L291H4

b CD4+ T cells

■ CCR4 (CD194)-BV421 Clone: 1G1
■ CCR4 (CD194)-BV421 Clone: L291H4

c

Lymphocytes

CCR7 (CD197)-PE
Clone: 3D12

Lymphocytes

CCR7 (CD197)-PE
Clone: G043H7

d CD4+ T cells

■ CCR7 (CD197)-PE Clone: 3D12
■ CCR7 (CD197)-PE Clone: G043H7

e

Monocytes

CD14-APC
Clone: Mφp9

Monocytes

CD14-BV421
Clone: MφP9

f

		B525	B690	Y585	Y610	Y763	R660	R712	R763	V450	V525	V610	Total Spread Given
FITC	B525		0.41	0.13	0.07	0.06	0.07	0.00	0.06	0.00	0.54	0.15	1.49
PerCP/Cy5.5	B690	0.15		0.00	0.10	0.67	0.28	1.69	0.66	0.00	0.00	0.00	3.54
PE	Y585	0.71	4.83		1.75	0.20	0.07	0.63	0.09	0.00	0.10	1.93	10.32
PE/CF594	Y610	0.16	6.08	1.43		0.36	0.00	0.76	0.05	0.00	0.00	1.40	10.24
PE/Cy7	Y763	0.36	1.11	0.85	0.39		0.25	0.22	1.82	0.00	0.00	0.20	5.20
APC	R660	0.00	0.80	0.01	0.24	1.05		2.38	1.48	0.09	0.00	0.11	6.16
AF700	R712	0.35	0.78	0.28	0.00	0.97	0.32		2.02	0.00	0.20	0.00	4.91
APC/Fire750	R763	0.00	0.20	0.00	0.00	1.90	0.84	0.90		0.00	0.00	0.00	3.84
BV421	V450	0.00	0.00	0.13	0.10	0.06	0.00	0.05	0.06		0.35	0.15	0.90
BV510	V525	0.18	0.36	0.46	0.92	0.00	0.00	0.00	0.24	0.79		1.25	4.20
BV605	V610	0.16	2.13	3.87	8.04	0.49	0.10	0.34	0.14	0.82	0.04		16.12
Total Spread Received		2.06	16.69	7.14	11.61	5.76	1.94	6.97	6.63	1.70	1.23	5.20	

◄**Fig. 1** Considerations of antibody clones and fluorochromes during panel development. **a–d** Comparison of different antibody clones for chemokine receptors detection on T cells. Plots showed CCR4 expression (**a, b**) and CCR7 expression (**c, d**) on CD4$^+$ cells. The CCR4 dim population and CCR7 dim population were clearly separated from the negative population when the CCR4-clone L291H4 and CCR7-clone G043H7 were used. **e** Brightness of fluorochromes is essential in the discrimination of immune cell subsets. Non-classical monocytes (CD14^{low} CD16^{hi}) could be identified when the bright (BV421) fluorochrome was used. **f** A representative spillover spreading matrix from an 11-color configuration of the CytoFLEX LX. The color coding was from no spillover spread (white) to high spillover spread (red). The three fluorophores contributing the least spillover spreading were BV421 (V450), FITC (B525), and PerCP/Cy5.5 (B690). In turn, the three detectors receiving the least spillover spreading are V525, V450, and R660

OMIPs	Optimized multicolor immunofluorescence panels
PBMCs	Peripheral blood mononuclear cells
PBS	Phosphate buffered saline
PD-1	Programmed cell death protein 1
pDCs	Plasmacytoid dendritic cells
PE	Phycoerythrin
PerCP	Peridinin–chlorophyll–protein complex
PFA	Paraformaldehyde
PMNs	Polymorphonuclear leukocytes
QC	Quality control
RCPs	Rainbow calibration particles
rCV	Robust coefficient of variance
RT	Room temperature
SBR	Signal-to-background ratio
SE	Spreading error
SI	Stain index
SOM	Self-organizing map
SPADE	Spanning-tree progression analysis of density-normalized events
SSC	Side scatter
SSM	Spillover spreading matrix
Tc cells	Cytotoxic T cells
Tconv cells	Conventional T cells
TCR	T cell receptor
Tfh cells	T follicular helper cells
Tfr cells	T follicular regulatory cells
Th cells	T helper cells
Treg cells	Regulatory T cells
TSCM cells	Stem memory T cells
t-SNE	t-distributed stochastic neighbor embedding

Introduction

The human immune system is a complex network of molecules, cells, and tissues that provide effective host defense. Due to its plasticity, the immune system is highly variable between individuals (Brodin and Davis 2017; Liston et al. 2016, 2021). A major aim of phenomics is to quantitatively measure these multiscale networks. Immunophenotyping is essential for analyzing the components and functions of the immune system. The standardized deep immunophenotyping approach will provide an opportunity for longitudinal monitoring of human immune status (Hartmann et al. 2019).

Multi-parametric flow cytometry is a rapidly developing technology that stands as one of the most important analytical tools in the field of immunology (Delmonte and Fleisher 2019). It allows the simultaneous identification and quantification of distinct immune cell subsets at a single-cell level. New antibodies, new fluorochromes, and high-performing flow cytometers are expanding the possibilities for the identification and phenotypic characterization of specific cell populations. However, the increased complexity of immunophenotypic approaches requires optimized antibody panels and fully standardized procedures (Maecker et al. 2010; Maecker et al. 2012).

Selection of Markers and Clones

The design of reproducible antibody panels to produce optimal resolution data for multi-parametric flow cytometry is laborious and time-consuming. As the first step in panel design, it is necessary to clarify the expression level (low to high), expression pattern (bimodal, continuum), and co-expression patterns of the target antigen. Typically, target antigens can be divided into two groups: lineage markers, and function markers. The lineage markers often have known expression patterns, which are used to delineate the target immune cell populations. The function markers are related to the process of cell biology such as cell proliferation, differentiation, activation and exhaustion with unknown expression patterns. An important issue for consideration is the selection of antibody clones. Different antibody clones against the same target antigen have distinct staining patterns from one another (Fig. 1a–d). There are several resources available to help choose commonly used, validated antibody clones such as the series of optimized multicolor immunofluorescence panels (OMIPs) publications (Wang and Creusot 2021) and the OMIP database (https://www.omipcollection.com).

Choice of Fluorochromes

Fluorochrome selection is an essential step in designing multicolor immunofluorescence panels. Different fluorochromes display a wide range of brightness scales. In general, bright fluorochromes (e.g., PE, BV421) should be reserved for function markers with low expression level, or unknown expression patterns. They can also be chosen for the continuum markers that require clear discrimination between dimly stained and negative cell populations. For example, BV421-conjugated CD14 antibody stained brightly and provided

good separation between intermediate monocytes and non-classical monocytes (Fig. 1e). While dim fluorochromes (i.e., FITC, PerCP/Cy5.5) can be assigned to lineage markers with high expression level such as CD3 and CD45.

Spillover Spreading Error

Spillover spreading has a critical impact on the quality of high-dimensional fluorescent antibody panels for flow cytometry (Nguyen et al. 2013). The signal from one fluorophore spilling into non-target detectors reduces the sensitivity of detectors. An important strategy to minimize spillover spreading is assigning the weak marker to the channel that receives less spread and assigning the backbone marker to the channel that contributes less spread. Figure 1f shows the spillover spreading matrix (SSM) of all possible combinations in the 11-color space for the CytoFLEX LX flow cytometer (Beckman Coulter).

Standardized Deep Immunophenotyping Workflow

For deep immunophenotyping of human peripheral whole blood, we developed and validated six different 11-color flow cytometry panels (Table 1). This assay characterizes immune cell subsets that circulate in the peripheral blood including all major immune cells such as neutrophils, eosinophils, basophils, monocytes, dendritic cells (DCs), natural killer (NK) cells, T cells, and B cells. It is suited for capturing thousands of immune cell traits including immune cell subset events, frequency, ratio, morphologic properties, and immune cell-surface protein expression levels.

The multi-step procedure must be standardized for flow cytometric immunophenotyping. These steps involve the instrument characterization (Nguyen et al. 2013; Perfetto et al. 2006, 2012), detector gain determination (Kalina et al. 2012; Maciorowski et al. 2017), antibody titration, sample staining (Berhanu et al. 2003), and data analysis (Monaco et al. 2016). Here, we describe in detail aspects of the procedures that are crucial for the deep immunophenotyping of human whole blood by multiparametric flow cytometry.

Materials and Methods

Materials and Reagents

Fresh human peripheral whole blood was collected in heparin-coated tubes or ethylenediaminetetraacetic acid (EDTA) anticoagulant tubes. All fluorochrome-conjugated antibodies used are listed in Supplementary Table S1. Whole blood samples were lysed with FACS™ Lysing Solution (BD, Cat#349202), and washed with phosphate buffered saline (PBS, Wisent, Cat#311-010-CL). After the final wash, cells were resuspended in paraformaldehyde (PFA; Sangon Biotech, Cat#A500684-0500). Eight-peaks Rainbow Calibration Particles (RCPs; Spherotech, Cat#RCP-30-5A), Anti-Mouse Ig, κ/Negative Control Compensation Particles Set (BD, Cat# 552843) were used in the procedures described in this protocol. All samples were acquired on a CytoFLEX LX Flow Cytometer (Beckman Coulter, Cat#C00446) through CytExpert_v2.4 (Beckman Coulter), and analyzed with FlowJo_v10.8.1 (BD). Data plots and statistical analyses

Table 1 Overview of the 6 panels for immunophenotyping of human whole blood

Laser	488 nm		561 nm			638 nm			405 nm		
Filter	525/40	690/50	585/42	610/20	763/43	660/20	712/25	763/43	450/45	525/40	610/20
Fluorochrome	FITC	PerCP/Cy5.5	PE	PE/CF594	PE/Cy7	APC	AF700	APC/Fire750	BV421	BV510	BV605
Panel 1: PMNs, monocytes and DCs panel											
Specificity	CD64	CD15	CD86	CD11c	CD123	CD16	HLA-DR	LIN[a]	CD14	CD45	CD38
Panel 2: NK, NKT, MAIT and γδT cells											
Specificity	TCR Vα7.2	NKp46	TCR Vδ2	NKG2D	CD16	TCR γδ	CD161	CD3	CD56	CD45	CD8
Panel 3: T eff/mem and Treg cells panel											
Specificity	CCR7	CD3	CD95	CD25	HLA-DR	CD39	CD45RA	CD4	CD127	CD45	CD8
Panel 4: T cells functional status panel											
Specificity	CD85j	CD3	PD-1	CD69	CD28	CD57	HLA-DR	CD4	CD38	CD45	CD8
Panel 5: Th, Tc, Tfh and Treg cells panel											
Specificity	CXCR5	CD3	ICOS	CD25	CXCR3	CCR6	CD127	CD4	CCR4	CD45	CD8
Panel 6: B cells panel											
Specificity	CD21	CD20	CD24	CD11c	IgD	CD38	IgG	CD19	CD27	CD45	IgM

FITC, fluorescein isothiocyanate; PE, phycoerythrin; PerCP, peridinin–chlorophyll–protein complex; Cy5.5, cyanine 5.5; Cy7, cyanine 7; APC, allophycocyanin; AF, Alexa Fluor; BV: Brilliant Violet. Eff/mem, effector/memory; LIN, lineage

[a]LIN includes CD3, CD19 and CD56

were done in FlowJo_v10.8.1 and Microsoft Excel_2016 (Microsoft Corporation).

Reagent Setup

- Stain buffer: PBS with 2% fetal bovine serum (FBS; Gibco, Cat#10099141) (vol/vol). Stain buffer can be stored at 2–8 °C for up to 2 weeks. Do not freeze.
- 1×Lysing Solution: Dilute the 10×concentrate FACS™ Lysing Solution 1:10 with ddH$_2$O at room temperature (RT, 20–25 °C).
- 1% PFA: Dilute the 4% PFA (Sangon Biotech, Cat#A500684-0500) 1:4 with PBS.
- Antibody premixes: Mix the correct concentration of the antibodies, as determined by titration experiments, to 20 µL of stain buffer per sample (chemokine receptor antibodies premix and surface-staining antibodies premix). Centrifuge before use at 14,000×g for 2 min at RT to remove antibodies aggregates.

Procedure

Instrument Characterization and Detector Gain Optimization

Calibration of Detector Linearity and Gain Range

1. Vortex the 8-peaks RCPs vigorously. Add 2–3 drops of particles to 1 mL of ddH$_2$O in a 5 mL 12×75 mm polypropylene tube.
2. Check CytoFLEX LX flow cytometer's lasers, mirrors, and filters. Complete daily instrument-specific start-up and quality control (QC) procedures.
3. Adjust the Forward scatter (FSC)/Side scatter (SSC) gain to place the beads on a scale in the light scatter plot and set a gate around the singlet cell population on the FSC-area (FSC-A) vs FSC-height (FSC-H) dot plot to exclude aggregates.
4. Set gains for all detectors to 25 V (Except FSC/SSC channel).
5. Run 8-peaks RCPs and negative control compensation particles (CCPs), respectively. Acquire 5000 events for each kind of particle.
6. Increase gain by 50 V for each detector and repeat Step 5.
7. Export data in FCS3.1 file format and load into FlowJo.
8. Calculate the median fluorescence intensity (MFI) of both the second brightest bead peak (referred to as P7_MFI) and the brightest bead peak (referred to as P8_MFI). Calculate the detector linearity as follows: linearity $= \frac{P8\_MFI - P7\_MFI}{P7\_MFI}$ (Fig. S1a).

9. Calculate the robust coefficient of variance (rCV) for the second brightest bead peak (referred to as P7_rCV).
10. Calculate the MFI of the negative CCPs and defined them as background (referred to as B_MFI). Calculate the signal-to-background ratio (SBR) as follows: SBR $= \frac{P7\_MFI}{B\_MFI}$ (Fig. S1a).
11. For each detector, plot the detector linearity, P7_rCV, and SBR on one graphic. Here the detector gain range can be defined as the gain point showing the highest SBR co-occurring with the lowest rCV and a slope of zero on the linearity curve (Fig. S1b).
12. Repeat this procedure when a new laser, detector, or filter is installed.

Calculation of Minimal Detector Gain

13. Gate the second dimmest peak of the 8-peaks RCPs and calculate the rCV of that peak (referred to as P2_rCV) in each fluorescence detector for gain ranges as described in the previous section.
14. Generate a plot showing the P2_rCV on the *y*-axis relative to the gain on the *x*-axis. When the slope of the curve is zero, the gain is minimal and brings the negative population out of the detector's electronic noise range (Fig. S1c).

> **CRITICAL**
>
> Gain titration to deliver optimal resolution (see supplementary optional procedure subheading Gain Titration (Voltration) Experiment).

Antibody Titration and Sample Staining

> **CRITICAL**
>
> 1. Human peripheral whole blood should be processed as soon as possible after collection.
> 2. Human peripheral whole blood should be transported and stored at RT.
> 3. For biosafety and to prevent sample contamination, whole blood samples should be processed in a biosafety cabinet.

Antibody Titration

15. Plan on using 120 µL/tube to stain, and a five-point, twofold dilution series.

16. Prepare five 200 μL cap tubes for each antibody. Label tubes with #1–#5 (4 dilutions and one unstained sample).

17. Transfer 32 μL stain buffer into cap tube #1, and add 8 μL of antibody. Mix thoroughly by a vortex.

18. Add 20 μL of stain buffer into cap tubes #2–#5.

19. Pipette 20 μL of antibody dilution from cap tube #1 into cap tube #2 and mix thoroughly by vortex.

20. Pipette 20 μL of antibody dilution from cap tube #2 into cap tube #3 and mix thoroughly by vortex.

21. Pipette 20 μL of antibody dilution from cap tube #3 into cap tube #4 and mix thoroughly by vortex.

22. Pipette 20 μL of antibody dilution from cap tube #4 and discard into waste.

23. Prepare five 5 mL 12 × 75 mm polypropylene tubes for each antibody. Label tubes with #1–#5 (4 dilutions and one unstained sample). And transfer 100 μL of whole blood into each polypropylene tube.

24. Transfer each antibody dilution into the corresponding 12 × 75 mm polypropylene tube. Mix thoroughly by a vortex. Thus, the antibody final concentrations are 1:30, 1:60, 1:120, 1:240, and 0, respectively.

25. For chemokine receptor antibodies, incubate for 15 min in a 37 °C water bath in the dark. For remaining surface-staining antibodies, incubate for 15 min at RT in the dark.

26. Add 2 mL 1 × Lysing Solution to each labelled 5 mL tube.

27. Mix thoroughly by vortex, and incubate for 15 min at RT in the dark.

28. Centrifuge the cells at $500 \times g$ for 5 min at RT.

29. Flick or aspirate to remove supernatant and wash cells with 2 mL PBS at $500 \times g$ for 5 min at RT.

30. Flick or aspirate to remove supernatant and wash twice.

31. Flick or aspirate to remove supernatant and resuspend in a final volume of 250 μL 1% PFA. Store at 2–8 °C and protect from light until acquisition. Do not freeze.

32. Check CytoFLEX LX flow cytometer's lasers, mirrors, and filters. Complete daily instrument-specific start-up and QC procedures.

33. Load the dilution series samples on the flow cytometer.

34. Adjust the FSC/SSC gain to place the cells on a scale in the light scatter plot and set a gate around the singlet cell population on the FSC-A vs FSC-H dot plot to exclude aggregates.

35. Adjust the detector gain determined with the previous procedure (see subheading Calculation of Minimal Detector Gain), and acquire 200 μL per sample.

36. Export data in FCS3.1 file format and load into FlowJo.

37. Calculate the stain index (SI) for each sample using the following formula: SI $= \frac{MFI(pos) - MFI(neg)}{2 \times rSD(neg)}$.

38. Generate a plot showing the SI on the y-axis relative to the dilution on the x-axis. The dilution that represents the best SI with the lowest concentration of antibody is the dilution to use (Fig. S2).

Compensation Setup Experiment

39. Vortex the BD CompBeads vigorously. In the meantime, label 5 mL 12 × 75 mm polypropylene tubes for each fluorochrome-conjugated antibody.

40. Pipette 80 μL of stain buffer into each tube and then add 20 μL of CompBeads (containing 10 μL positive control beads, along with 10 μL negative control beads).

41. Add the correct concentration of the antibodies to each tube, which is determined by the titration experiments (see subheading Antibody Titration).

42. Prepare one additional tube as a negative control (without any antibody).

43. Mix thoroughly by vortex, and incubate for 15 min at RT in the dark.

44. Add 2 mL stain buffer to each tube.

45. Centrifuge the cells at $500 \times g$ for 5 min at RT.

46. Flick or aspirate to remove supernatant and resuspend in a final volume of 250 μL stain buffer. Store at 4 °C and protect from light and moisture until acquisition. Do not freeze.

47. Check CytoFLEX LX flow cytometer's lasers, mirrors, and filters. Complete daily instrument-specific start-up and QC procedures.

48. Create a new compensation experiment, and select the channel requiring compensation calculation and the sample type.

49. Adjust the FSC/SSC gain to place the BD CompBeads on a scale in the light scatter plot and set a gate around the singlet cell population on the FSC-A vs FSC-H dot plot to exclude aggregates.

50. Adjust the detector gain determined with the previous procedure (see subheading Calculation of Minimal Detector Gain).

51. Load one of the single-stained samples, and acquire 5000 events per tube.

52. Repeat Step 13 for all single-stained samples.

53. Check all acquired samples, and move the positive or negative gates in the plot to define the target population.

54. Click the "Compensation Calculation" button to generate the compensation matrix.

CRITICAL

1. Carefully check the origin of the antibody. The BD CompBeads Anti-Mouse Ig, κ particles, which bind mouse κ light chain-bearing immunoglobulin. Vendors such as Invitrogen and BioLegend provide compensation beads that can bind with antibodies of mouse, rat, hamster, rabbit, and human origin.
2. If compensation beads are not available at the time that can bind antibodies of rat or hamster origin, the original antibody can be replaced with an antibody of the same fluorochrome.
3. Routinely performing the compensation setup experiment.
4. Characterization of spillover spreading error (SE) to reveal fluorescence spectrum interactions (see supplementary optional procedure subheading Spillover Spreading Matrix Determination Experiment).

Whole Blood Staining Procedures

55. Prepare 5 mL 12×75 mm polypropylene tubes for each panel, and label tubes with the name of the panel.
56. Transfer 100 µL of whole blood into each labelled 5 mL tube.
57. Spin shortly (about 20 s) all antibody premixes.
58. For panel 1, 2, 3 and 4, proceed to procedures 59–66, for panel 5, skip procedures 59–66 and proceed to procedures 67–76, and for panel 6, skip procedures 59–76 and proceed to procedures 77–86.

For Panel 1, 2, 3 and 4

59. Add each antibody premix to the corresponding tube.
60. Mix thoroughly by vortex, and incubate for 15 min at RT in the dark.
61. Add 2 mL 1×Lysing Solution to each labelled 5 mL tube.
62. Mix thoroughly by vortex, and incubate for 15 min at RT in the dark.
63. Centrifuge the cells at $500 \times g$ for 5 min at RT.
64. Flick or aspirate to remove supernatant and wash cells with 2 mL PBS at $500 \times g$ for 5 min at RT.
65. Flick or aspirate to remove supernatant and wash twice.
66. Flick or aspirate to remove supernatant and resuspend in a final volume of 250 µL 1% PFA. Store at 2–8 °C and protect from light until acquisition. Do not freeze.

For Panel 5

67. Add chemokine receptor antibodies premix in the corresponding tube.
68. Mix thoroughly by vortex, and incubate for 15 min in a 37 °C water bath in the dark.
69. Add remaining surface-staining antibodies premix in the corresponding tube.
70. Mix thoroughly by vortex, and incubate for 15 min at RT in the dark.
71. Add 2 mL 1×Lysing Solution to the corresponding tube.
72. Mix thoroughly by vortex, and incubate for 15 min at RT in the dark.
73. Centrifuge the cells at $500 \times g$ for 5 min at RT.
74. Flick or aspirate to remove supernatant and wash cells with 2 mL PBS at $500 \times g$ for 5 min at RT.
75. Flick or aspirate to remove supernatant and wash twice.
76. Flick or aspirate to remove supernatant and resuspend in a final volume of 250 µL 1% PFA. Store at 2–8 °C and protect from light until acquisition. Do not freeze.

CRITICAL

If necessary, prepare three times 100 µL of whole blood stained in parallel and pooled directly before measurement to obtain sufficient cell numbers.

For Panel 6

77. Add 2 mL 1×Lysing Solution to the corresponding tube.
78. Mix thoroughly by vortex, and incubate for 15 min at RT in the dark.
79. Centrifuge the cells at $500 \times g$ for 5 min at RT.
80. Flick or aspirate to remove supernatant and wash cells with 2 mL PBS at $500 \times g$ for 5 min at RT.
81. Flick or aspirate to remove supernatant and resuspend in 100 µL stain buffer.
82. Add Panel-6 antibodies premix in the corresponding tube.
83. Mix thoroughly by vortex, and incubate for 15 min at RT in the dark.
84. Add 2 mL PBS to the corresponding tube, and mix thoroughly by the vortex.
85. Centrifuge the cells at $500 \times g$ for 5 min at RT.

86. Flick or aspirate to remove supernatant and resuspend in a final volume of 250 μL 1% PFA. Store at 2–8 °C and protect from light until acquisition. Do not freeze.

> **CRITICAL**
>
> If necessary, prepare three times 100 μL of whole blood stained in parallel and pooled directly before measurement to obtain sufficient cell numbers.

Data Acquisition and Quality Checks

Data Acquisition

87. Check CytoFLEX LX flow cytometer's lasers, mirrors, and filters. Complete daily instrument-specific start-up and QC procedures.
88. Before the acquisition, lasers should warm up for 15 min.
89. Adjust the FSC/SSC gain to place the cells on a scale in the light scatter plot and set a gate around the singlet cell population on the FSC-A vs FSC-H dot plot to exclude aggregates.
90. Adjust the detector gain determined with the previous procedure (see subheading Calculation of Minimal Detector Gain).
91. Acquire samples (200 μL per panel per sample) using CytExpert at a high flow rate (60 μL/min). And it is recommended to acquire more than 200,000 events per sample.

Compensation Quality Check

92. Load FCS3.1 files into CytExpert, which is software that controls the CytoFLEX LX flow cytometer operation.
93. Apply the compensation matrix generated with the previous procedure (see subheading Preparation of compensation controls).
94. Create N-by-N bivariate plots of all combinations to check the current sample's fluorescent parameters compensation.
95. When the compensation matrix is not suitable, check the following three items: (1) the single-stained compensation controls should be matched to the correct detectors; (2) positive and negative populations should be correctly determined by the gates in each control; (3) no contamination occurred during the preparation of the single-stained samples.
96. Further manual adjustment of the compensation is required if any of the compensation is not proper.

Data Cleaning

97. Install the "FlowAI" Plugin in FlowJo (see the Installing Plugins page for details: https://docs.flowjo.com/flowjo/plugins-2/installing-plugins/).
98. Load the FCS3.1 files into FlowJo which have been checked the compensation.
99. Access and initiate FlowAI via the Plugins Menu in FlowJo (Workspace Tab—> Populations Band—> Plugins menu) to remove any anomalies. And select cleaned data for the next step of data analysis.
100. Set a gate around the singlet cell population on the FSC-A vs FSC-H dot plot and FSC-width (FSC-W) vs FSC-A dot plot to exclude aggregates.
101. Clean up the data based on the number of immune cell subsets after manual gating by setting the limits of detection (LOD) to > 20 cells and the lower limit of quantification (LLOQ) to > 50 cells. A population of cells with fewer than 50 cells in 80% of samples is filtered out.

Troubleshooting

Problem	Possible reason	Potential solution
rCVs on either the 8-peaks RCPs or negative CCPs are greater in one detector than another detector	Dichroic steering mirror is out of alignment	Adjust the steering mirror alignment
Detector's linearity curve does not reach a plateau	Detector is faulty or poorly aligned	Replace the detector
rCVs on the 8-peaks RCPs increase with gain setting series	Detector is faulty	Replace the detector
SI curve does not reach a plateau in the voltration experiment	Voltration process does not reach a maximal resolution	Continue the voltration process at higher gain setting series
Positive compensation beads with the specific fluorochrome-conjugated antibody are negative	The antibody is incompatible with the bead	Species-specific antibody compensation beads should be used
Poorly discriminate the positive population from the negative population	Antibodies were not used at optimal concentrations, or staining method was not optimized for chemokine receptor antibodies	Titrate all antibodies before experiments, or stain with chemokine receptor antibodies at 37 °C

Problem	Possible reason	Potential solution
Many combinations are undercompensated or overcompensated	The signal of the positive compensation control was not as bright as the whole blood sample	Use whole blood samples for the compensation control
Interruptions during acquisition (visualized via the time parameter)	Instability of flow stream	Resuspend cells to exclude aggregates and exclude the events with flowAI

Anticipated Results

Polymorphonuclear Leukocytes (PMNs), Monocytes, and DCs

To characterize major subsets of innate immune cells, CD45^{+} cells were identified after the exclusion of doublets (Fig. 2a). We include the marker CD16 to differentiate eosinophils from neutrophils among the CD15^{+} population (Fig. 2b) (Gustafson et al. 2015; Patin et al. 2018; Ruhle et al. 2016). The basophils were identified as HLA-DR^{−} CD123^{+} cells on lineage (CD3/CD14/CD19/CD56) negative population. The lineage^{−} HLA-DR^{+} population was further distinguished into myeloid dendritic cells (mDCs) and plasmacytoid dendritic cells (pDCs) according to their differential expression of CD11c and CD123. (Fig. 2d) (Mair and Prlic 2018; Park et al. 2020). Monocytes are early responders to pathogens in acute infections. The monocytes were discriminate different inflammatory/differentiation stages by their CD14 and CD16 expression: classical monocytes (CD14^{hi} CD16^{−}), intermediate monocytes (CD14^{hi} CD16^{+}) and non-classical monocytes (CD14^{+} CD16^{hi}) (Fig. 2c) (Bocsi et al. 2014; Hally et al. 2022; Park et al. 2020; Staser et al. 2018). The expressions of CD64, CD86, CD38, and HLA-DR can be evaluated to determine the activation state of the PMNs, monocytes, and DCs (Fig. 2e).
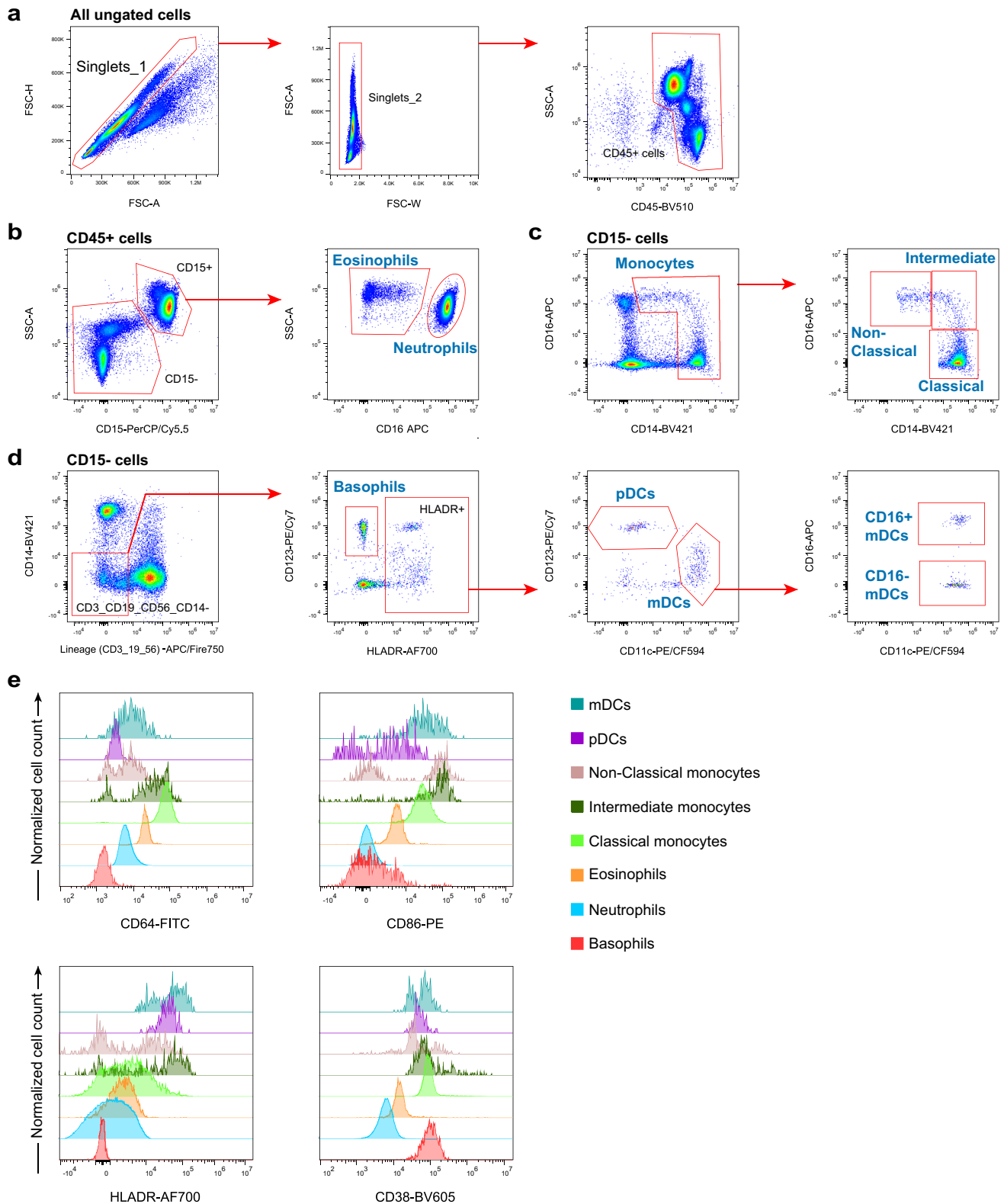
Unconventional T Cells and NK Cells

The unconventional T cells are a diverse group of relatively rare lymphocytes which play important roles in disease (Bae et al. 2018; Godfrey et al. 2019, 2018, 2016; Mayassi et al. 2021; Petley et al. 2021; Silva-Santos et al. 2019; Wilkinson and Cerrone 2020). Lymphocytes were distinguished into CD3^{+} and CD3^{−} populations (Fig. 3a). We identified γδ T cells and their subsets on CD3^{+} T cells by markers TCR γδ and TCR Vδ2 (Fig. 3b) (Gherardin et al. 2014; Hertoghs et al. 2020; Mahnke et al. 2013c). The mucosal-associated invariant T (MAIT) cells were identified by their CD161^{+} TCR Vα7.2^{+} phenotype in total T cells (Fig. 3c) and αβ

cells, CD8^{+} T cells and CD8^{−} T cells (Fig. 3d) (Gherardin et al. 2014; Hertoghs et al. 2020). NK cells have a strong cytolytic function against virus-infected cells. We included CD56 as common NK cell marker to identify NK and NKT cells (Fig. 3e, g) (Costanzo et al. 2015; Eller and Currier 2012; Hertoghs et al. 2020; Mahnke et al. 2013c). NKT cells are further identified in αβ cells, CD8^{+} T cells and CD8^{−} T cells (Fig. 3f). Previous studies have shown the presence of NK cells that do not express CD56, especially in the peripheral blood of patients with chronic viral infections (Bjorkstrom et al. 2010). Therefore, we also provide a gating strategy to identify NK cells as CD3^{−} NKp46^{+} (Fig. 3h) (Park et al. 2020; Patin et al. 2018). Additional two activating receptors (NKG2D and NKp46) distribution among different cell subsets were evaluated (Fig. 3i).

T Cell Subsets

T cells are important mediators in cell-mediated immunity, and numerous different T cell subsets were identified and characterized. To identify T cells the pan marker CD3 was included in panels 2, 3, 4, and 5. CD4^{+} T cells, CD8^{+} T cells, the double-negative T cells (CD4^{−} CD8^{−} T cells), and double-positive T cells (CD4^{+} CD8^{+} T cells) were identified by their differential CD4 and CD8 expression (Fig. 4a). The CD8^{+} T cells (Fig. 4b) and CD4^{+} T cells (Fig. 4c) were further distinguished into naïve T cells (CD45RA^{+} CCR7^{+} CD95^{−}), stem memory T cells (TSCM, CD45RA^{+} CCR7^{+} CD95^{+}), effector T cells (CD45RA^{+} CCR7^{−}), effector memory T cells (EM, CD45RA^{−} CCR7^{−}), and central memory T cells (CM, CD45RA^{−} CCR7^{+}) by their CD45RA, CCR7 and CD95 expression level (Mahnke et al. 2012; Staser et al. 2018). The expression levels of surface markers (CD95, CD39, and HLA-DR) of T cells at different stages of maturation were further evaluated. The regulatory T cells (Tregs) were identified by their CD25^{hi} CD127^{−/low} phenotype on CD4^{+} T cells and the activation status was determined by the markers CD45RA and HLA-DR (Fig. 4d) (Biancotto et al. 2012; Liechti and Roederer 2019b; Mahnke et al. 2013a; Murdoch et al. 2012; Park et al. 2020). And Treg subpopulations were analyzed for the CD39 activation marker expression. In addition, the conventional T (Tconv) cells were identified and further distinguished into different maturation stages in Fig. 4e.

To determine the activation status of T cells and their subsets (CD4^{+} T cells, CD8^{+} T cells, CD4^{−} CD8^{−} T cells, and CD4^{+} CD8^{+} T cells), the expression of activation markers CD69, CD28, HLA-DR, and CD38 was analyzed in Panel 4 (Fig. 5a). The inhibitory receptor (CD85j), exhaustion marker programmed cell death protein 1 (PD-1), and senescence marker CD57 expression was also examined in these T cell subsets (Fig. 5b) (Healy and Murdoch 2016;

a All ungated cells

Singlets_1

Singlets_2

CD45+ cells

b CD45+ cells

CD15+
CD15-

Eosinophils
Neutrophils

c CD15- cells

Monocytes

Intermediate
Non-Classical
Classical

d CD15- cells

CD3_CD19_CD56_CD14-

Basophils
HLADR+

pDCs
mDCs

CD16+ mDCs
CD16- mDCs

e

Normalized cell count

CD64-FITC

CD86-PE

HLADR-AF700

CD38-BV605

- mDCs
- pDCs
- Non-Classical monocytes
- Intermediate monocytes
- Classical monocytes
- Eosinophils
- Neutrophils
- Basophils

Swanson and Seder 2020). CD85j$^+$ T cells have been shown to be associated with aging (Alpert et al. 2019). The PD-1 is upregulated after T cell activation to prevent an excessive immune response. The CD57 was a marker of terminal differentiation and associated with autoimmune diseases, infectious diseases, and cancer (Characiejus et al. 2008; Palmer et al. 2005; Pedroza-Seres et al. 2007).

◄**Fig. 2** Gating strategies for the PMNs, Monocytes and DCs panel (Panel 1). **a** CD45⁺ cells were identified by their CD45 expression after exclusion of doublets by cross-checking the forward scatter (FSC) signal for its area (A) versus height (H) and width (W) characteristics. **b** CD45⁺ leukocytes were distinguished into CD15⁺ and CD15⁻ populations, then neutrophils and eosinophils were identified by their CD16 expression on CD15⁺ cells. **c** Identification of monocytes. Total monocytes were separated on an CD14 versus CD16 dot plot from CD15⁻ SSC^low cells. Monocytes were identified and further distinguished into classical monocytes (CD14^hi CD16⁻), intermediate monocytes (CD14^hi CD16⁺) and non-classical monocytes (CD14⁺ CD16^hi) by their CD14 and CD16 expression. **d** Identification of basophils and dendritic cells. Lineage negative cells were identified by their expression of CD3, CD14, CD19 and CD56. Then the basophils (HLA-DR⁻ CD123⁺) were gated on an anti-HLA-DR versus anti-CD123 dot plot. mDCs (CD11c⁺ CD123⁻) and pDC (CD11c⁻ CD123⁺) were identified by their differential CD11c and CD123 expression. The mDCs were further subdivided into CD16⁺ mDC and CD16⁻ mDC by their CD16 expression. **e** Expression of functional markers (CD69, CD28, HLA-DR, and CD38) by different PMNs, monocytes, and DCs subsets. A reference population of CD3⁻ CD56⁻ cells from the same sample was served as a negative expression control. Basophils can be used as a negative expression control for CD64, CD86, and HLA-DR

In Panel 5 the CD4⁺ T cells were further distinguished into the Th1 (CXCR3⁺ CCR4⁻ CCR6⁻), Th2 (CXCR3⁻ CCR4⁺ CCR6⁻), Th9 (CCR4⁻ CCR6⁺), Th17 (CXCR3⁻ CCR4 + CCR6⁺), and Th17/Th1 (CXCR3⁺ CCR4⁻ CCR6⁺) (Fig. 6a) (Mahnke et al. 2013b). T follicular helper (Tfh) cells, T follicular regulatory (Tfr) cells, and CXCR5⁺ CD8⁺ T cells were identified by their expression of CXCR5 (Fig. 6b–d). In addition, different Th-like subsets were identified based on the expression of CXCR3, CCR4, and CCR6 for Tfh cells (Fig. 6e), Treg cells (Fig. 6f), and cytotoxic T (Tc) cells (Fig. 6g), with similar gating strategies for Th cells (Brodie et al. 2013; Swieboda et al. 2019; Wingender and Kronenberg 2015). CD278 is a CD28-superfamily costimulatory molecule expressed on activated T cells, also known as inducible T-cell costimulator (ICOS), which was included to further characterize the functional status of individual subsets (Fig. 6h).

B Cell Subsets

To identify total B cells, two B cell pan markers CD19 and CD20 were included in panel 6 (Fig. 7a). CD21^−/low B cells were identified in Fig. 7b, which represent an innate-like B cell population (Rakhmanov et al. 2009). CD11c⁺ memory B cells were gated on total B cells (Fig. 7c), which are precursors of antibody-secreting cells (Golinski et al. 2020). The CD27⁺ memory B cells, naïve B cells, transitional B cells, and founder B cells were characterized in a two-step process by their expression of IgD, CD27, CD38, and CD24 (Fig. 7d). In addition, we identified unswitched B cells, marginal zone B cells, IgD only memory B cells, and IgM only memory B cells based on their differential expression of IgD

and IgM (Fig. 7e). Plasmablasts, plasma cells, and class-switched B cells were identified from IgD⁻ IgM⁻ B cells (Fig. 7f). The gating strategies for B cell subsets presented here refer to the studies of OMIP-003 (Wei et al. 2011), OMIP-047 (Liechti et al. 2018), OMIP-051 (Liechti and Roederer 2019a), and OMIP-068 (Cascino et al. 2020).

Discussion

Understanding the phenotypes of human immune system is important to define metrics of immunological health. Here, we present a standardized workflow for high-dimensional single-cell immunophenotyping of human whole blood using multi-parametric flow cytometry. Our six optimized panels can also be freely combined with other panels for specific hypothesis-driven studies. The researchers can replicate the procedures easily and avoid costly, time-consuming mistakes during panel development. The robust platform approach of using high-throughput flow cytometry can be applied to biological and medical research.

Our panels enable deep phenotyping of most of the immune cell populations in human peripheral blood. Several groups have designed multicolor flow cytometry panels for the monitoring of immune cells from peripheral blood mononuclear cells (PBMCs) (Moncunill et al. 2014; Nogimori et al. 2021; Park et al. 2020; Payne et al. 2020). However, polymorphonuclear leukocytes such as granulocytes are depleted in PBMCs. Granulocytes are important components of the human innate immune system. The identification of granulocytes including neutrophils, eosinophils and basophils was designed in our assay. Our panels also included the assessment of unconventional T cells (γδ T cells, NKT cells, MAIT cells). Unconventional T cells share functional profiles of both innate and adaptive immunity that play critical roles in many diseases (Bae et al. 2018; Feng et al. 2015; Godfrey et al. 2019, 2018, 2016; Mayassi et al. 2021; Petley et al. 2021; Silva-Santos et al. 2019; Wilkinson and Cerrone 2020). It is important to understand the immune functional status of the unconventional T cells. Furthermore, we identified different Th and Th-like subsets by their expression of CXCR3, CCR4, and CCR6 on classical Th cells, Tfh cells, Tregs, and Tc cells. These designed panels enable us to capture thousands of immune cell traits.

Flow cytometry is a powerful tool that provides rapid multi-parametric analysis of cells at the single-cell level. Additional standardization efforts are also needed in the selection of reagents, instrument setup, sample handling, and data analysis to decrease variability in a longitudinal study or multi-site study (Gratama et al. 2002; Gratama et al. 1997; Kalina 2020; Maecker et al. 2010; Maecker et al. 2012). Several international consortia are developing standardization of flow cytometry protocols and applications such as
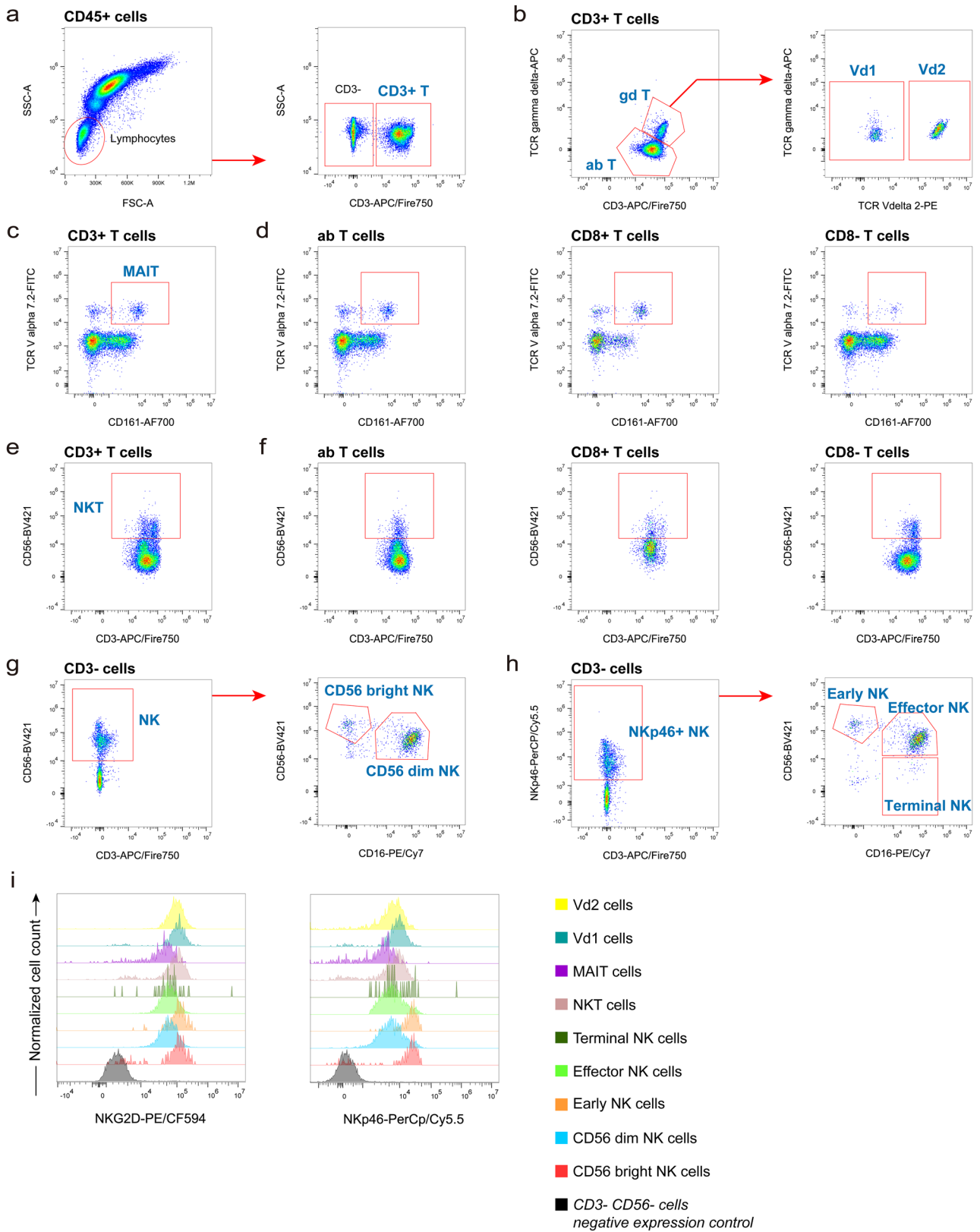
◄Fig. 3 Gating strategies for the NK, NKT, MAIT and γδ T cells panel (Panel 2). Exclusion of doublets and gating of CD45+ cells as shown for panel 1 (Fig. 2a). **a** Lymphocytes were gated on the FSC-A versus SSC-A dot plot, and T cells were identified by their CD3 expression. **b** Identification of αβ T cells and γδ T cells (anti-CD3 versus anti-TCR γδ plot). The γδ T cells were further subdivided into Vδ1 cells and Vδ2 cells (anti-TCR Vδ2 versus anti-TCR γδ plot). **c** Identification of MAIT cells (anti-CD161 versus anti-TCR Vα7.2 plot) and MAIT cells in αβ cells, CD8+ T cells and CD8− T cells (**d**). **e** Identification of NKT cells (anti-CD3 versus anti-CD56 plot) and NKT cells in αβ cells, CD8+ T cells and CD8− T cells (**f**). **g, h** Two gating strategies to identify NK cells. NK cells can be determined by CD3− CD56+ cells (**e**) and subsequently distinguished into two subsets by their CD56 and CD16 co-expression into CD56 bright NK cells (CD56^{hi} CD16$^{−/low}$) and CD56 dim NK cells (CD56^{low} CD16+). NK cells can also be determined by CD3− NKp46+ cells (**f**), which were divided into early NK cells (CD56^{hi} CD16$^{−/low}$), effector NK cells (CD56^{low} CD16+) and terminal NK cells (CD56− CD16+). **i** Expression of activating receptors (NKG2D and NKp46) by different cell subsets

the EuroFlow Consortium (Kalina et al. 2012; van Dongen et al. 2012), the ONE study consortium (Streitz et al. 2013), the Human Immunology Project Consortium (HIPC) (Brusic et al. 2014; Courtot et al. 2015; Finak et al. 2016; Maecker et al. 2012), the PRECISAIDS project (Jamin et al. 2016), and several other groups (Hasan et al. 2015; Ivison et al. 2018). There are a variety of aims for these projects, and the focuses of standardization differ. These studies provided a reference framework for standardized flow cytometry and inspired our research.

Establishing robust flow cytometry panels requires careful selection of antibody clones and fluorochrome combinations. For researchers starting Panel design, ranking target antigens is a good place to start. Antigen ranking should mainly consider the following three points, including (1) the expression level of the target antigen on the cells of interest, antigens with low expression levels should be given priority; (2) the required resolution of the target antigen, specifically, for functional markers, which usually expression occur along a continuum and therefore need to be considered first, while for lineage markers (e.g. CD3, CD4, etc.), which usually have good separation pattern, can be considered later; and (3) gating strategies, the markers in the back of the gating order should be noted to prevent the influence of the preceding markers. Based on the above antigen ranking, further fluorochromes selection and testing are performed. We conducted extensive antibody testing (we presented a few examples of antibody selection in the Fig. 1) and found significantly different performances of antibody reagents from different suppliers. We suggest choosing suitable antibodies from different suppliers according to the testing results. For instrument setup, we describe the optimized methods based on existing data and experience. Usually, it is subjective to adjust the voltage gains based on the unstained sample. We describe a practical procedure on how to set the optimal

voltage gains for each fluorescence detector (Maecker and Trotter 2006; Perfetto et al. 2006, 2012). Furthermore, we noticed the compensation by software automated algorithms needs to be carefully reviewed, and if necessary, adjusted compensation after sample acquisition.

This protocol was optimized for direct staining of human peripheral blood samples which is time-saving and minimizes variations in sample preparation. The procedures for previous studies on immunophenotyping assays were including isolation of PBMCs, freezing and thawing cells. However, several studies have demonstrated that the isolation of PBMCs by Ficoll density gradient centrifugation will alter the expression of cell surface markers, cell subset distribution and function (Appay et al. 2006; Hoffmeister et al. 2003; Maecker et al. 2012, 2005; Renzi and Ginns 1987; Valle et al. 2012). It can also include additional variations owing to freezing/thawing steps. Our immunophenotyping assay was developed for an easy, fast procedure in only 2 mL of human peripheral blood.

Manual gating of flow cytometry data is a major source of variability in flow cytometry analyses. Our gating strategy was designed for batch analysis using FlowJo and minimized the gating adjustment. It is well suited for centralized data analysis (Maecker et al. 2005). Recently the advances in computational flow cytometry make it possible to further explore multiparametric flow cytometry data using high-dimensional analysis methods, such as t-distributed stochastic neighbor embedding (t-SNE) (van der Maaten and Hinton 2008), viSNE (Amir el al. 2013), Spanning-tree progression analysis of density-normalized events (SPADE) (Qiu et al. 2017), FlowSOM (Van Gassen et al. 2015), FLOW-MAP (Zunder et al. 2015), and PhenoGraph (Levine et al. 2015). These computational methods will be more efficient, objective and have better reproducibility (Brummelman et al. 2019; Mair et al. 2016; Saeys et al. 2016). However, there are several challenges that need to be solved such as automated population identification, mapping cell types across samples, etc. (Saeys et al. 2016).

In conclusion, we present six multi-parametric flow cytometry panels for the deep immunophenotyping of human whole blood. The standardized approach and protocols for instrument setup, antibody titration, sample staining, and data quality checks were described. However, this protocol is not designed to investigate the secreted proteins and intracellular proteins of the immune cells such as cytokines, and transcriptional factors. The deep immunophenotyping approach can generate a high informative value of datasets. These huge and high-dimensional data can be analyzed by computational flow cytometry methods. Computational flow cytometry is emerging as an important new field for profiling immunity in humans. It will promote a deeper understanding of the complex heterogeneity of cellular
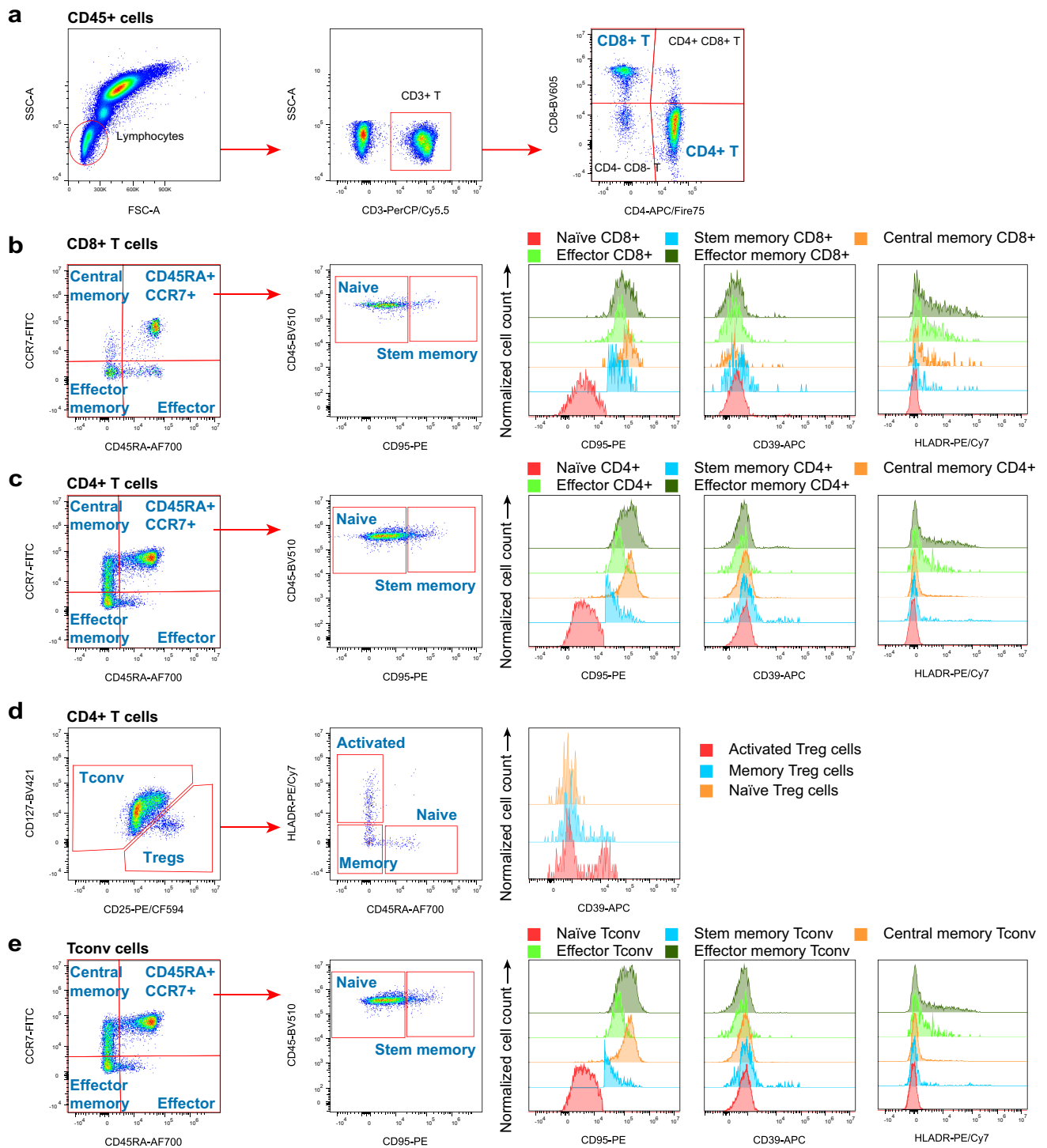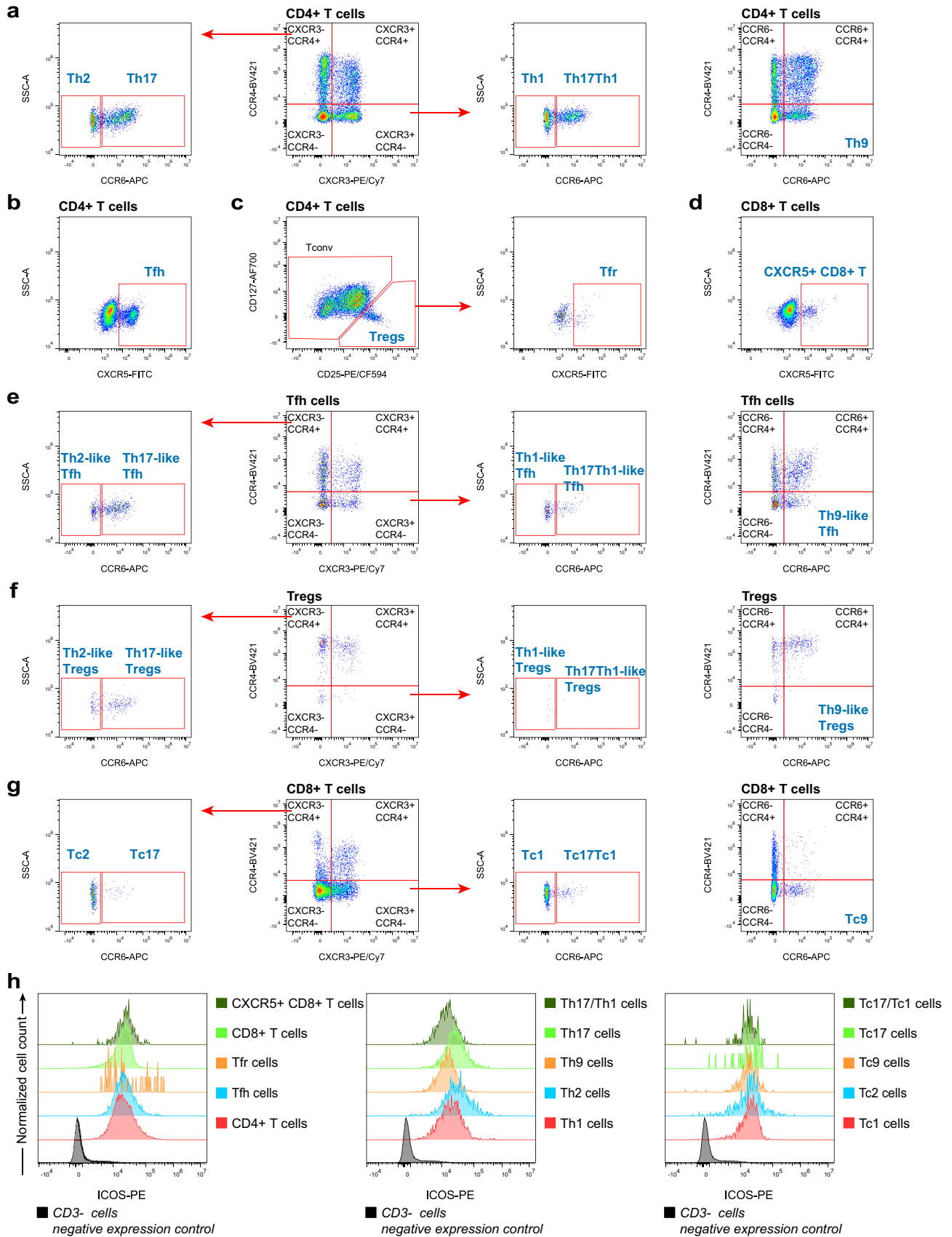
Fig. 4 Gating strategies for the T eff/mem and Treg cells panel (Panel 3). Exclusion of doublets and gating of $CD45^+$ cells as shown for panel 1 (Fig. 2a). **a** Lymphocytes were gated on the FSC-A versus SSC-A dot plot, and T cells were identified by their CD3 expression. $CD4^+$ T cells, the double-negative T cells ($CD4^-$ $CD8^-$ T cells), $CD8^+$ T cells, and double-positive T cells ($CD4^+$ $CD8^+$ T cells) were identified by their expression of CD4 and CD8. **b, c** Identification of different maturation stages of $CD8^+$ T cells (**b**) and $CD4^+$ T cells (**c**). Naïve T cells ($CD45RA^+$ $CCR7^+$ $CD95^-$), stem memory T cells ($CD45RA^+$ $CCR7^+$ $CD95^+$), effector T cells ($CD45RA^+$ $CCR7^-$), effector memory T cells ($CD45RA^-$ $CCR7^-$), and central memory T

cells ($CD45RA^-$ $CCR7^+$) were identified by their expression levels of CD45RA, CCR7 and CD95. The expression levels of surface markers (CD95, CD39, and HLA-DR) of T cells at different stages of maturation were further evaluated. **d** Tconv and Treg cells were identified by their expression of CD25 and CD127. Treg cells were further distinguished into $CD45RA^-$ $HLA-DR^+$ activated, $CD45RA^-$ $HLA-DR^-$ memory, and $CD45RA^+$ $HLA-DR^-$ naïve regulatory T cells. Treg subpopulations were analyzed for the CD39 activation marker expression. **e** Identification of different stages of Tconv cells and analysis of surface markers
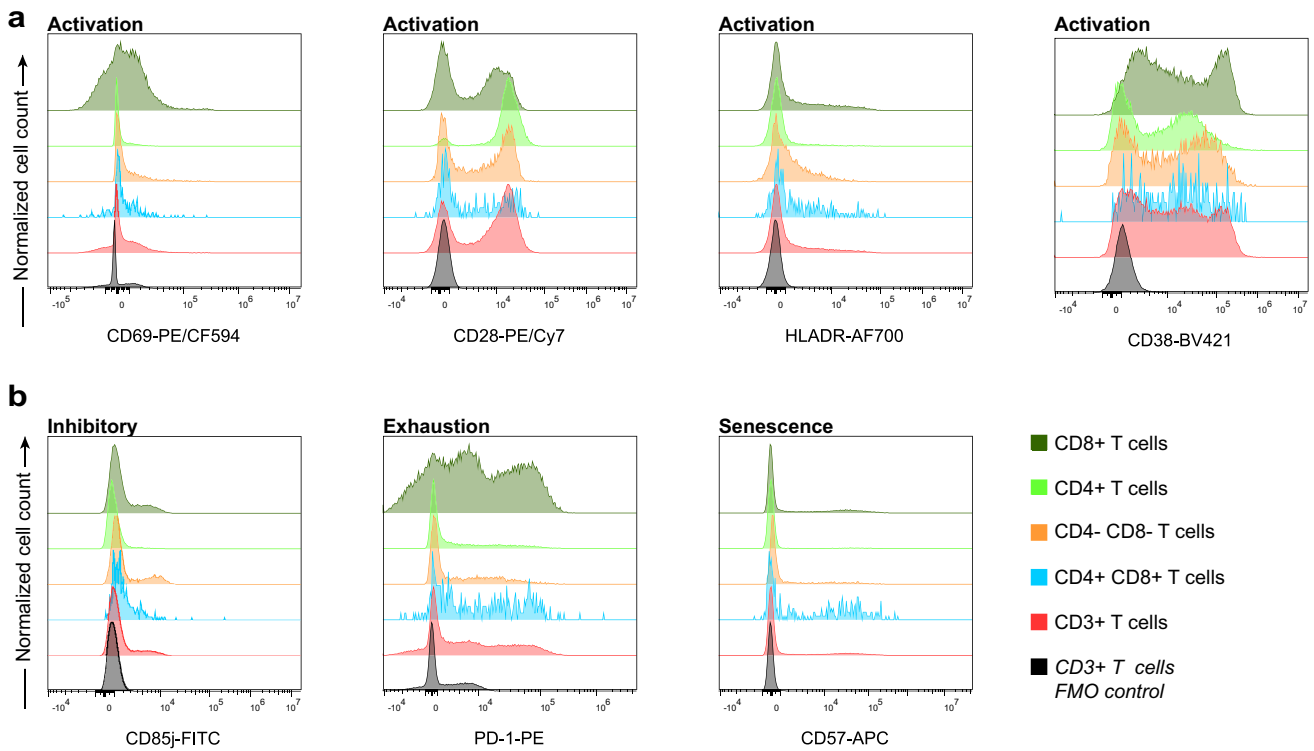
Fig. 5 Expression of activation, inhibitory and exhaustion markers by different T cell subsets (T cell functional status panel, Panel 4). Exclusion of doublets and gating of CD45$^+$ cells as shown for panel 1 (Fig. 2a). CD4$^+$ T cells, CD8$^+$ T cells, CD4$^-$ CD8$^-$ T cells, and CD4$^+$ CD8$^+$ T cells were identified by their expression of CD4 and CD8 (shown in Fig. 4a). **a** Expression of activation markers (CD69, CD28, HLA-DR, and CD38) by different T cell subsets. **b** Expression of the inhibitory receptor (CD85j), exhaustion marker PD-1, and terminal differentiation marker CD57 by different T cell subsets. Lower histograms represent the fluorescence minus one (FMO) control expression for the lineage-gated CD3$^+$ T cells. FMO controls for the functional markers were performed on one whole blood sample

◄**Fig. 6** Gating strategies for the Th, Tc, Tfh and Treg cells panel (Panel 5). Exclusion of doublets and gating of CD45$^+$ cells as shown for panel 1 (Fig. 2a). CD4$^+$ T cells, CD8$^+$ T cells, CD4$^-$ CD8$^-$ T cells, and CD4$^+$ CD8$^+$ T cells were identified by their expression of CD4 and CD8 (shown in Fig. 4a). **a** Identification of the Th subsets. Th1 (CXCR3$^+$ CCR4$^-$ CCR6$^-$), Th2 (CXCR3$^-$ CCR4$^+$ CCR6$^-$), Th9 (CCR4$^-$ CCR6$^+$), Th17 (CXCR3$^-$ CCR4$+$CCR6$^+$), and Th17/Th1 (CXCR3$^+$ CCR4$^-$ CCR6$^+$) subsets are identified on CD4$^+$ T cells as indicated. **b** Tfh cells were identified on the anti-CXCR5 versus SSC-A plot. **c** CD4$^+$ T cells were divided into Tconv cells and Treg cells, which were subsequently distinguished into CXCR5$^+$ Tfr cells (anti-CXCR5 versus SSC-A plot). **d** CXCR5$^+$ CD8$^+$ T cells were gated on the anti-CXCR5 versus SSC-A plot. **e–g** Different Th-like subsets were identified based on the expression of CXCR3, CCR4, and CCR6 for Tfh cells (**e**), Treg cells (**f**), and Tc cells (**g**) with similar gating strategies for Th cells. **h** The expression levels of ICOS of different T cell subsets were evaluated. A reference population of CD3$^-$ cells from the same sample was served as a negative expression control

behaviors, individual disease states, and perturbations of human immune system.

Author Contributions JG and FQ designed and coordinated the study. JG, YL, HL, YZ, JZ, XH, JH and HL performed experiments. JG and FQ contributed to scientific discussion. JG and FQ wrote the first draft of the manuscript. All authors reviewed, revised, and approved the final manuscript.
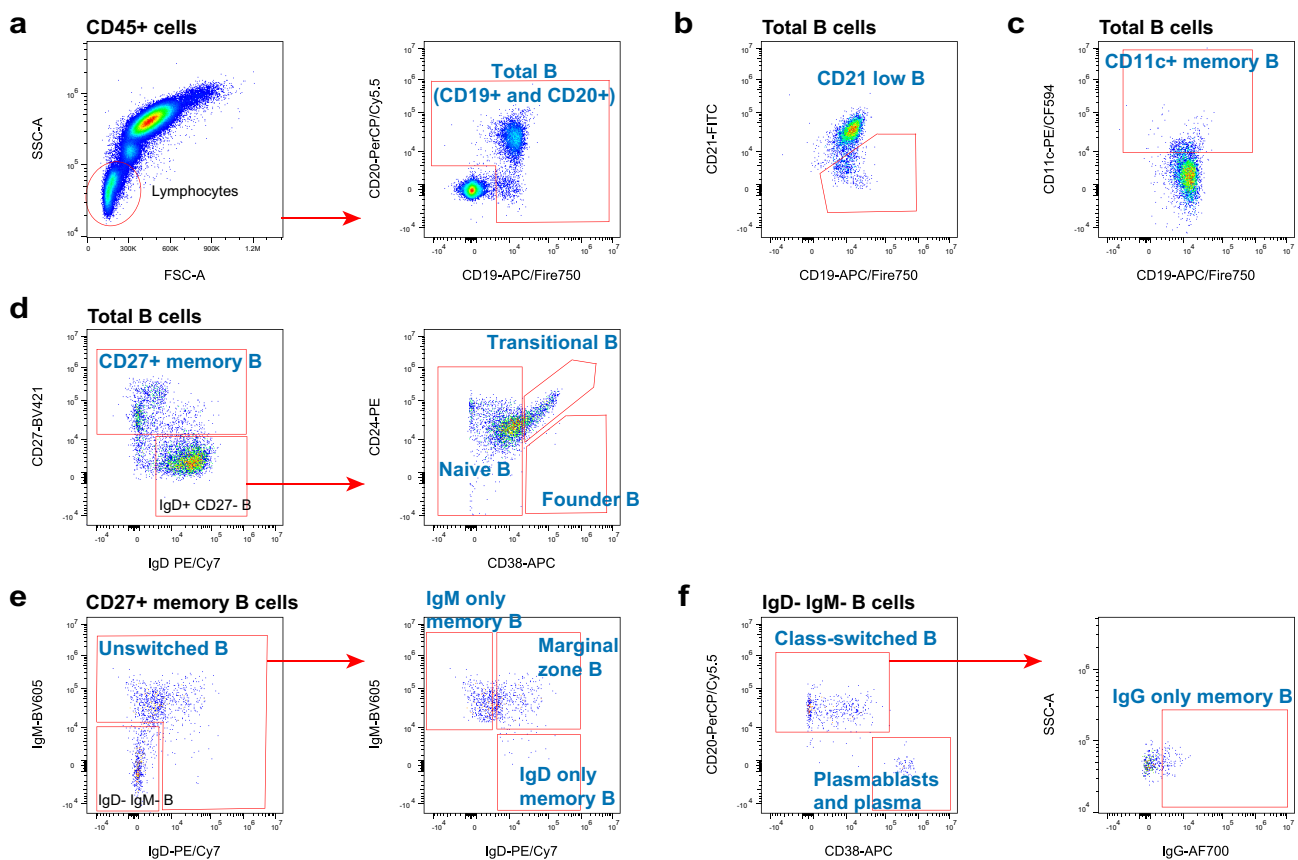

Fig. 7 Gating strategies for the B cells panel (Panel 6). Exclusion of doublets and gating of CD45$^+$ cells as shown for panel 1 (Fig. 2a). **a** Lymphocytes were gated on the FSC-A versus SSC-A dot plot, and total B cells (CD19$^+$ and CD20$^+$) were identified on an anti-CD19 versus anti-CD20 dot plot for subsequent analyses. **b** CD21$^{-/low}$ B cells (anti-CD19 versus anti-CD21 plot) were identified on total B cells. **c** CD11c$^+$ memory B cells (anti-CD19 versus anti-CD11c plot) were identified on total B cells. **d** The subsets CD27$^+$ memory B cells, naïve B cells, transitional B cells, and founder B cells were characterized in a two-step process by their expression of IgD, CD27, CD38, and CD24. **e** CD27$^+$ memory B cells were further divided into unswitched B cells and IgD$^-$ IgM$^-$ B cells. Marginal zone B cells, IgD only memory B cells, and IgM only memory B cells were evaluated on the anti-IgD versus anti-IgM plot. **f** Plasmablasts, plasma cells and class-switched B cells (anti-CD38 versus anti-CD20 plot) were identified on IgD$^-$ IgM$^-$ B cells. The class-switched B cells were further gated for IgG only memory B cells (anti-IgG versus SSC-A plot)

Data Availability The datasets generated during and/or analyzed during the current study are available from the corresponding author on reasonable request.

Declarations

Conflict of interest The authors declare that they have no conflict of interest.

Consent to participate All the participants provided informed consent.

Consent for publication Not applicable.

Ethics approval The study was approved by the Institutional Review Board of School of Life Science, Fudan University.

References

Alpert A, Pickman Y, Leipold M et al (2019) A clinically meaningful metric of immune age derived from high-dimensional longitudinal monitoring. Nat Med 25(3):487–495. https://doi.org/10.1038/s41591-019-0381-y

Appay V, Reynard S, Voelter V et al (2006) Immuno-monitoring of CD8+ T cells in whole blood versus PBMC samples. J Immunol Methods 309(1–2):192–199. https://doi.org/10.1016/j.jim.2005.11.007

Bae EA, Seo H, Kim BS et al (2018) Activation of NKT cells in an anti-PD-1-resistant tumor model enhances antitumor immunity by reinvigorating exhausted CD8 T cells. Cancer Res 78(18):5315–5326. https://doi.org/10.1158/0008-5472.CAN-18-0734

Berhanu D, Mortari F, De Rosa SC et al (2003) Optimized lymphocyte isolation methods for analysis of chemokine receptor expression. J Immunol Methods 279(1–2):199–207. https://doi.org/10.1016/s0022-1759(03)00186-8

Biancotto A, Dagur PK, Fuchs JC et al (2012) OMIP-004: in-depth characterization of human T regulatory cells. Cytometry A 81(1):15–16. https://doi.org/10.1002/cyto.a.21158

Bjorkstrom NK, Ljunggren HG, Sandberg JK (2010) CD56 negative NK cells: origin, function, and role in chronic viral disease. Trends Immunol 31(11):401–406. https://doi.org/10.1016/j.it.2010.08.003

Bocsi J, Melzer S, Dahnert I et al (2014) OMIP-023: 10-color, 13 antibody panel for in-depth phenotyping of human peripheral blood leukocytes. Cytometry A 85(9):781–784. https://doi.org/10.1002/cyto.a.22505

Brodie T, Brenna E, Sallusto F (2013) OMIP-018: chemokine receptor expression on human T helper cells. Cytometry A 83(6):530–532. https://doi.org/10.1002/cyto.a.22278

Brodin P, Davis MM (2017) Human immune system variation. Nat Rev Immunol 17(1):21–29. https://doi.org/10.1038/nri.2016.125

Brummelman J, Haftmann C, Nunez NG et al (2019) Development, application and computational analysis of high-dimensional fluorescent antibody panels for single-cell flow cytometry. Nat Protoc 14(7):1946–1969. https://doi.org/10.1038/s41596-019-0166-2

Brusic V, Gottardo R, Kleinstein SH et al (2014) Computational resources for high-dimensional immune analysis from the Human Immunology Project Consortium. Nat Biotechnol 32(2):146–148. https://doi.org/10.1038/nbt.2777

Cascino K, Roederer M, Liechti T (2020) OMIP-068: high-dimensional characterization of global and antigen-specific B cells in chronic infection. Cytometry A 97(10):1037–1043. https://doi.org/10.1002/cyto.a.24204

Characiejus D, Ukoniene VP, Auskaite RJ et al (2008) Peripheral blood CD8highCD57+ lymphocyte levels may predict outcome in melanoma patients treated with adjuvant interferon-alpha. Anticancer Res 28(2b):1139–1142

Costanzo MC, Creegan M, Lal KG et al (2015) OMIP-027: functional analysis of human natural killer cells. Cytometry A 87(9):803–805. https://doi.org/10.1002/cyto.a.22719

Courtot M, Meskas J, Diehl AD et al (2015) FlowCL: ontology-based cell population labelling in flow cytometry. Bioinformatics 31(8):1337–1339. https://doi.org/10.1093/bioinformatics/btu807

Delmonte OM, Fleisher TA (2019) Flow cytometry: surface markers and beyond. J Allergy Clin Immunol 143(2):528–537. https://doi.org/10.1016/j.jaci.2018.08.011

el Amir AD, Davis KL, Tadmor MD et al (2013) viSNE enables visualization of high dimensional single-cell data and reveals phenotypic heterogeneity of leukemia. Nat Biotechnol 31(6):545–552. https://doi.org/10.1038/nbt.2594

Eller MA, Currier JR (2012) OMIP-007: phenotypic analysis of human natural killer cells. Cytometry A 81(6):447–449. https://doi.org/10.1002/cyto.a.22033

Feng Y, van der Veeken J, Shugay M et al (2015) A mechanism for expansion of regulatory T-cell repertoire and its role in self-tolerance. Nature 528(7580):132–136. https://doi.org/10.1038/nature16141

Finak G, Langweiler M, Jaimes M et al (2016) Standardizing flow cytometry immunophenotyping analysis from the human immunophenotyping consortium. Sci Rep 6:20686. https://doi.org/10.1038/srep20686

Gherardin NA, Ritchie DS, Godfrey DI et al (2014) OMIP-021: simultaneous quantification of human conventional and innate-like T-cell subsets. Cytometry A 85(7):573–575. https://doi.org/10.1002/cyto.a.22475

Godfrey DI, Uldrich AP, McCluskey J et al (2016) Corrigendum: the burgeoning family of unconventional T cells. Nat Immunol 17(4):469. https://doi.org/10.1038/ni0416-469a

Godfrey DI, Le Nours J, Andrews DM et al (2018) Unconventional T cell targets for cancer immunotherapy. Immunity 48(3):453–473. https://doi.org/10.1016/j.immuni.2018.03.009

Godfrey DI, Koay HF, McCluskey J et al (2019) The biology and functional importance of MAIT cells. Nat Immunol 20(9):1110–1128. https://doi.org/10.1038/s41590-019-0444-8

Golinski ML, Demeules M, Derambure C et al (2020) CD11c(+) B cells are mainly memory cells, precursors of antibody secreting cells in healthy donors. Front Immunol 11:32. https://doi.org/10.3389/fimmu.2020.00032

Gratama JW, Kraan J, Van den Beemd R et al (1997) Analysis of variation in results of flow cytometric lymphocyte immunophenotyping in a multicenter study. Cytometry 30(4):166–177. https://doi.org/10.1002/(sici)1097-0320(19970815)30:4%3c166::aid-cyto2%3e3.0.co;2-i

Gratama JW, Kraan J, Keeney M et al (2002) Reduction of variation in T-cell subset enumeration among 55 laboratories using single-platform, three or four-color flow cytometry based on CD45 and SSC-based gating of lymphocytes. Cytometry 50(2):92–101. https://doi.org/10.1002/cyto.10084

Gustafson MP, Lin Y, Maas ML et al (2015) A method for identification and analysis of non-overlapping myeloid immunophenotypes in humans. PLoS ONE 10(3):e0121546. https://doi.org/10.1371/journal.pone.0121546

Hally KE, Ferrer-Font L, Pilkington KR et al (2022) OMIP 083: a 21-marker 18-color flow cytometry panel for in-depth phenotyping of human peripheral monocytes. Cytometry A 101(5):374–379. https://doi.org/10.1002/cyto.a.24545

Hartmann FJ, Babdor J, Gherardini PF et al (2019) Comprehensive immune monitoring of clinical trials to advance human immunotherapy. Cell Rep 28(3):819–831. https://doi.org/10.1016/j.celrep.2019.06.049

Hasan M, Beitz B, Rouilly V et al (2015) Semi-automated and standardized cytometric procedures for multi-panel and multi-parametric whole blood immunophenotyping. Clin Immunol 157(2):261–276. https://doi.org/10.1016/j.clim.2014.12.008

Healy ZR, Murdoch DM (2016) OMIP-036: co-inhibitory receptor (immune checkpoint) expression analysis in human T cell subsets. Cytometry A 89(10):889–892. https://doi.org/10.1002/cyto.a.22938

Hertoghs N, Schwedhelm KV, Stuart KD et al (2020) OMIP-064: a 27-color flow cytometry panel to detect and characterize human NK cells and other innate lymphoid cell subsets, MAIT cells, and gammadelta T cells. Cytometry A 97(10):1019–1023. https://doi.org/10.1002/cyto.a.24031

Hoffmeister B, Bunde T, Rudawsky IM et al (2003) Detection of antigen-specific T cells by cytokine flow cytometry: the use of whole blood may underestimate frequencies. Eur J Immunol 33(12):3484–3492. https://doi.org/10.1002/eji.200324223

Ivison S, Malek M, Garcia RV et al (2018) A standardized immune phenotyping and automated data analysis platform for multi-center biomarker studies. JCI Insight. https://doi.org/10.1172/jci.insight.121867

Jamin C, Le Lann L, Alvarez-Errico D et al (2016) Multi-center harmonization of flow cytometers in the context of the European "PRECISESADS" project. Autoimmun Rev 15(11):1038–1045. https://doi.org/10.1016/j.autrev.2016.07.034

Kalina T (2020) Reproducibility of flow cytometry through standardization: opportunities and challenges. Cytometry A 97(2):137–147. https://doi.org/10.1002/cyto.a.23901

Kalina T, Flores-Montero J, van der Velden VH et al (2012) EuroFlow standardization of flow cytometer instrument settings and immunophenotyping protocols. Leukemia 26(9):1986–2010. https://doi.org/10.1038/leu.2012.122

Levine JH, Simonds EF, Bendall SC et al (2015) Data-driven phenotypic dissection of AML reveals progenitor-like cells that correlate with prognosis. Cell 162(1):184–197. https://doi.org/10.1016/j.cell.2015.05.047

Liechti T, Roederer M (2019a) OMIP-051-28-color flow cytometry panel to characterize B cells and myeloid cells. Cytometry A 95(2):150–155. https://doi.org/10.1002/cyto.a.23689

Liechti T, Roederer M (2019b) OMIP-060: 30-parameter flow cytometry panel to assess T cell effector functions and regulatory T cells. Cytometry A 95(11):1129–1134. https://doi.org/10.1002/cyto.a.23853

Liechti T, Gunthard HF, Trkola A (2018) OMIP-047: high-dimensional phenotypic characterization of B cells. Cytometry A 93(6):592–596. https://doi.org/10.1002/cyto.a.23488

Liston A, Carr EJ, Linterman MA (2016) Shaping variation in the human immune system. Trends Immunol 37(10):637–646. https://doi.org/10.1016/j.it.2016.08.002

Liston A, Humblet-Baron S, Duffy D et al (2021) Human immune diversity: from evolution to modernity. Nat Immunol 22(12):1479–1489. https://doi.org/10.1038/s41590-021-01058-1

Maciorowski Z, Chattopadhyay PK, Jain P (2017) Basic multicolor flow cytometry. Curr Protoc Immunol 117:541–543. https://doi.org/10.1002/cpim.26

Maecker HT, Trotter J (2006) Flow cytometry controls, instrument setup, and the determination of positivity. Cytometry A 69(9):1037–1042. https://doi.org/10.1002/cyto.a.20333

Maecker HT, Rinfret A, D'Souza P et al (2005) Standardization of cytokine flow cytometry assays. BMC Immunol 6:13. https://doi.org/10.1186/1471-2172-6-13

Maecker HT, McCoy JP, Nussenblatt R (2012) Standardizing immunophenotyping for the human immunology project. Nat Rev Immunol 12(3):191–200. https://doi.org/10.1038/nri3158

Maecker HT, McCoy JP Jr, Consortium FHI et al (2010) A model for harmonizing flow cytometry in clinical trials. Nat Immunol 11(11):975–978. https://doi.org/10.1038/ni1110-975

Mahnke YD, Beddall MH, Roederer M (2012) OMIP-013: differentiation of human T-cells. Cytometry A 81(11):935–936. https://doi.org/10.1002/cyto.a.22201

Mahnke YD, Beddall MH, Roederer M (2013a) OMIP-015: human regulatory and activated T-cells without intracellular staining. Cytometry A 83(2):179–181. https://doi.org/10.1002/cyto.a.22230

Mahnke YD, Beddall MH, Roederer M (2013b) OMIP-017: human CD4(+) helper T-cell subsets including follicular helper cells. Cytometry A 83(5):439–440. https://doi.org/10.1002/cyto.a.22269

Mahnke YD, Beddall MH, Roederer M (2013c) OMIP-019: quantification of human gamma delta T-cells, iNKT-cells, and hematopoietic precursors. Cytom Part A 83(8):676–678. https://doi.org/10.1002/cyto.22326

Mair F, Prlic M (2018) OMIP-044: 28-color immunophenotyping of the human dendritic cell compartment. Cytometry A 93(4):402–405. https://doi.org/10.1002/cyto.a.23331

Mair F, Hartmann FJ, Mrdjen D et al (2016) The end of gating? An introduction to automated analysis of high dimensional cytometry data. Eur J Immunol 46(1):34–43. https://doi.org/10.1002/eji.201545774

Mayassi T, Barreiro LB, Rossjohn J et al (2021) A multilayered immune system through the lens of unconventional T cells. Nature 595(7868):501–510. https://doi.org/10.1038/s41586-021-03578-0

Monaco G, Chen H, Poidinger M et al (2016) flowAI: automatic and interactive anomaly discerning tools for flow cytometry data. Bioinformatics 32(16):2473–2480. https://doi.org/10.1093/bioinformatics/btw191

Moncunill G, Han HN, Dobano C et al (2014) OMIP-024: pan-leukocyte immunophenotypic characterization of PBMC subsets in human samples. Cytom Part A 85(12):995–998. https://doi.org/10.1002/cyto.a.22580

Murdoch DM, Staats JS, Weinhold KJ (2012) OMIP-006: phenotypic subset analysis of human T regulatory cells via polychromatic flow cytometry. Cytometry A 81(4):281–283. https://doi.org/10.1002/cyto.a.22024

Nguyen R, Perfetto S, Mahnke YD et al (2013) Quantifying spillover spreading for comparing instrument performance and aiding in multicolor panel design. Cytometry A 83(3):306–315. https://doi.org/10.1002/cyto.a.22251

Nogimori T, Sugawara Y, Higashiguchi M et al (2021) OMIP 078: A 31-parameter panel for comprehensive immunophenotyping of multiple immune cells in human peripheral blood mononuclear cells. Cytometry A 99(9):893–898. https://doi.org/10.1002/cyto.a.24490

Palmer BE, Blyveis N, Fontenot AP et al (2005) Functional and phenotypic characterization of CD57+ CD4+ T cells and their association with HIV-1-induced T cell dysfunction. J Immunol

175(12):8415–8423. https://doi.org/10.4049/jimmunol.175.12.8415

Park LM, Lannigan J, Jaimes MC (2020) OMIP-069: forty-color full spectrum flow cytometry panel for deep immunophenotyping of major cell subsets in human peripheral blood. Cytometry A 97(10):1044–1051. https://doi.org/10.1002/cyto.a.24213

Patin E, Hasan M, Bergstedt J et al (2018) Natural variation in the parameters of innate immune cells is preferentially driven by genetic factors. Nat Immunol 19(3):302–314. https://doi.org/10.1038/s41590-018-0049-7

Payne K, Li W, Salomon R et al (2020) OMIP-063: 28-color flow cytometry panel for broad human immunophenotyping. Cytometry A 97(8):777–781. https://doi.org/10.1002/cyto.a.24018

Pedroza-Seres M, Linares M, Voorduin S et al (2007) Pars planitis is associated with an increased frequency of effector-memory CD57+ T cells. Br J Ophthalmol 91(10):1393–1398. https://doi.org/10.1136/bjo.2007.116277

Perfetto SP, Ambrozak D, Nguyen R et al (2006) Quality assurance for polychromatic flow cytometry. Nat Protoc 1(3):1522–1530. https://doi.org/10.1038/nprot.2006.250

Perfetto SP, Ambrozak D, Nguyen R et al (2012) Quality assurance for polychromatic flow cytometry using a suite of calibration beads. Nat Protoc 7(12):2067–2079. https://doi.org/10.1038/nprot.2012.126

Petley EV, Koay HF, Henderson MA et al (2021) MAIT cells regulate NK cell-mediated tumor immunity. Nat Commun 12(1):4746. https://doi.org/10.1038/s41467-021-25009-4

Qiu X, Mao Q, Tang Y et al (2017) Reversed graph embedding resolves complex single-cell trajectories. Nat Methods 14(10):979–982. https://doi.org/10.1038/nmeth.4402

Rakhmanov M, Keller B, Gutenberger S et al (2009) Circulating CD21 low B cells in common variable immunodeficiency resemble tissue homing, innate-like B cells. Proc Natl Acad Sci USA 106(32):13451–13456. https://doi.org/10.1073/pnas.0901984106

Renzi P, Ginns LC (1987) Analysis of T cell subsets in normal adults. Comparison of whole blood lysis technique to Ficoll–Hypaque separation by flow cytometry. J Immunol Methods 98(1):53–56. https://doi.org/10.1016/0022-1759(87)90434-0

Ruhle PF, Fietkau R, Gaipl US et al (2016) Development of a modular assay for detailed immunophenotyping of peripheral human whole blood samples by multicolor flow cytometry. Int J Mol Sci. https://doi.org/10.3390/ijms17081316

Saeys Y, Van Gassen S, Lambrecht BN (2016) Computational flow cytometry: helping to make sense of high-dimensional immunology data. Nat Rev Immunol 16(7):449–462. https://doi.org/10.1038/nri.2016.56

Silva-Santos B, Mensurado S, Coffelt SB (2019) gammadelta T cells: pleiotropic immune effectors with therapeutic potential in cancer. Nat Rev Cancer 19(7):392–404. https://doi.org/10.1038/s41568-019-0153-5

Staser KW, Eades W, Choi J et al (2018) OMIP-042: 21-color flow cytometry to comprehensively immunophenotype major lymphocyte and myeloid subsets in human peripheral blood. Cytometry A 93(2):186–189. https://doi.org/10.1002/cyto.a.23303

Streitz M, Miloud T, Kapinsky M et al (2013) Standardization of whole blood immune phenotype monitoring for clinical trials: panels and methods from the ONE study. Transplant Res 2(1):17. https://doi.org/10.1186/2047-1440-2-17

Swanson PA 2nd, Seder RA (2020) OMIP-067: 28-color flow cytometry panel to evaluate human T-cell phenotype and function. Cytometry A 97(10):1032–1036. https://doi.org/10.1002/cyto.a.24189

Swieboda D, Guo Y, Sagawe S et al (2019) OMIP-062: a 14-color, 16-antibody panel for immunophenotyping human innate lymphoid, myeloid and T cells in small volumes of whole blood and pediatric airway samples. Cytometry A 95(12):1231–1235. https://doi.org/10.1002/cyto.a.23907

Valle A, Maugeri N, Manfredi AA et al (2012) Standardization in flow cytometry: correct sample handling as a priority. Nat Rev Immunol 12(12):864. https://doi.org/10.1038/nri3158-c3

van der Maaten L, Hinton G (2008) Visualizing data using t-SNE. J Mach Learn Res 9:2579–2605

van Dongen JJ, Lhermitte L, Bottcher S et al (2012) EuroFlow antibody panels for standardized n-dimensional flow cytometric immunophenotyping of normal, reactive and malignant leukocytes. Leukemia 26(9):1908–1975. https://doi.org/10.1038/leu.2012.120

Van Gassen S, Callebaut B, Van Helden MJ et al (2015) FlowSOM: using self-organizing maps for visualization and interpretation of cytometry data. Cytometry A 87(7):636–645. https://doi.org/10.1002/cyto.a.22625

Wang W, Creusot RJ (2021) Orchestrating multiplexity in polychromatic science through OMIPs: a decade-old resource to empower biomedical research. Cytometry A 99(9):866–874. https://doi.org/10.1002/cyto.a.24471

Wei C, Jung J, Sanz I (2011) OMIP-003: phenotypic analysis of human memory B cells. Cytometry A 79(11):894–896. https://doi.org/10.1002/cyto.a.21112

Wilkinson KA, Cerrone M (2020) Targeting unconventional T cells for vaccination against tuberculosis. Am J Respir Cell Mol Biol 62(4):401–402. https://doi.org/10.1165/rcmb.2019-0403ED

Wingender G, Kronenberg M (2015) OMIP-030: characterization of human T cell subsets via surface markers. Cytometry A 87(12):1067–1069. https://doi.org/10.1002/cyto.a.22788

Zunder ER, Lujan E, Goltsev Y et al (2015) A continuous molecular roadmap to iPSC reprogramming through progression analysis of single-cell mass cytometry. Cell Stem Cell 16(3):323–337. https://doi.org/10.1016/j.stem.2015.01.015